Inter-subject cerebrovascular variability: a source of uncertainty for dose calculation to circulating blood cells for glioblastoma patients treated with modern radiotherapy techniques

IOP Publishing Phys. Med. Biol. 69 (2024) 175010 https://doi.org/10.1088/1361-6560/ad69f9

Physics in Medicine & Biology

IPEM Institute of Physics and Engineering in Medicine

OPEN ACCESS

RECEIVED
13 June 2024

REVISED
17 July 2024

ACCEPTED FOR PUBLICATION
31 July 2024

PUBLISHED
21 August 2024

PAPER

Inter-subject cerebrovascular variability: a source of uncertainty for dose calculation to circulating blood cells for glioblastoma patients treated with modern radiotherapy techniques

Abdelkhalek Hammi[1,*], **Nadya Shusharina**[2,3] **and Sonya Djuffouo**[1]

[1] Physics Department, TU University, Dortmund, Germany
[2] Division of Radiation Biophysics, Department of Radiation Oncology, Massachusetts General Hospital, Boston, MA 02114, United States of America
[3] Harvard Medical School, Boston, MA 02115, United States of America
[*] Author to whom any correspondence should be addressed.

E-mail: abdelkhalek.hammi@tu-dortmund.de

Keywords: circulating blood cells, dose uncertainty, intersubject variation, brain vasculature, VMAT and IMRT, glioblastoma

Abstract

Purpose. To assess how inter-subject variations in brain vasculature among glioblastoma (GBM) patients affects the calculated dose received by circulating blood cells (CBC) during radiotherapy and its subsequent impact on CBC depletion. *Methods.* Ten GBM patients treated with either intensity-modulated radiation therapy (IMRT) or volumetric modulated arc therapy (VMAT) were selected. For each patient, 23 cerebrovascular models were developed based on 23 healthy subject MR-angiography data to simulate intra- and inter-subject blood vessel diversity. Based on the corresponding treatment plan of the patient, the dose to CBC was calculated for all the 230 scenarios. The impact of inter-subject variation on fraction of irradiated blood volume ($V_{D>0\ \mathrm{cGy}}$) and lymphocyte kill rates as a function of the clinical target volume (CTV) size and treatment technique were analyzed. *Results.* The dose fluctuation to CBC was higher in IMRT plans compared to VMAT plans. The uncertainty in the $V_{D>0\ \mathrm{cGy}}$ was 18.3% for IMRT and 2.0% ($\mathrm{CI}_{95\%}$) for VMAT and the dispersion of the $D_{2\%}$ index was 6 cGy for IMRT and 1 cGy for VMAT ($\mathrm{CI}_{95\%}$) for one single treatment fraction of 200 cGy. The uncertainty in killed CBC due to inter-subject diversity in brain blood vessel increased with increasing CTV size and was $\sigma = 11.2\%$. *Conclusions.* VMAT showed greater robustness against inter-subject variation in blood vessels compared to IMRT. We recommend considering the uncertainty in depleting CBC resulting from the use of less patient-specific and generic blood vessel phantoms to improve the radiation-induced lymphopenia assessments.

1. Introduction

Glioblastomas (GBM) are the most common type of adult brain tumor, comprising approximately 78% of all malignant primary brain tumors (Ostrom *et al* 2017, Ilic and Ilic 2023). More than 40% of gliomas patients, treated with combined temozolomide and radiotherapy, suffered from prolonged radiation-induced lymphopenia (RiL) (Grossman *et al* 2015), which persists for up to 12 months after finishing radiotherapy and is associated with reduced survival (Pillay *et al* 2013, Razavi *et al* 2016, Byun 2019, Kim *et al* 2019, Kleinberg *et al* 2019, Song 2021).

The growing recognition of the link between RiL and poor survival outcomes for GBM patients underscores the crucial role of the immune systemin their survival (Saeed 2024). This significant association highlights the potential for improving GBM patient outcomes by mitigating RiL. Currently, there is no consensus on dosimetric constraints for circulating immune blood cells (CBC) to mitigate RiL. Therefore, accurate estimation of the accumulated dose to CBC from treatment plans is essential to develop effective mitigation strategies. This could help establish the connection between treatment plan configurations (such

as treatment technique, dose rates, fractionation and fraction treatment time) and the risk of developing RiL over the course of fractionated treatment.

In brain tumor patients, accurate dose calculation to CBCs is particularly challenging due to the absence of lymphatic tissue and the fact that these immune cells primarily circulate through the bloodstream (Mapunda *et al* 2022), making them difficult to delineate. Consequently, the morphology and location of an individual patient's brain vessels within the radiation field directly impact the estimated dose to the CBCs flowing through these vessels, potentially confounding the risk assessment for developing RiL.

Direct observation of cerebral blood vessels from standard imaging techniques like CT or MRI is challenging, requiring advanced imaging methods (e.g. angiography) and intensive labor to delineate them. Therefore, studies simulating the dose to CBC often use approximation models and less patient-specific blood vessel phantoms adaptable to the organ (Yovino *et al* 2013, Basler *et al* 2018, Jin *et al* 2020, Shin *et al* 2021). In a previous study (Hammi *et al* 2020), we developed a generic cerebral vessel phantom to mimic blood flow through the radiation field. Large blood vessels were manually segmented from MRI data. However, this generic model does not accurately reflect individual patient-specific blood vessel configurations, adding uncertainty to CBC dose estimation.

To address this limitation, Hammi (2023) hypothesized that major brain arteries and veins are located near the folds and grooves of the cerebral cortex (Shalom *et al* 2021, Vachha *et al* 2022), and proposed an image processing method to extract these topographic characteristics from standard T1 and T2 MRI images and trace the surface vessels. This method allows for the development of more patient-specific blood vessel models; however, it is limited to surface vessels and is less effective for deep-located large vessels such anterior cerebral arteries (ACAs) due to the lack of topographic features within the brain.

The human cerebrovascular system has a complex network of branches and connections between arteries and veins (Daneman and Prat 2015). While the topography of major brain vessels is consistent across individuals (Wright *et al* 2013), the branching patterns vary among different demographic and racial groups (Yang *et al* 2022). Additionally, brain blood vessels continuously remodel based on physiological needs or due to cancer (Tregub *et al* 2022). Therefore, to improve the accuracy of RiL assessment in brain cancer patients, understanding the impact of inter-subject vascular diversity on dosimetric uncertainty for CBCs is crucial, especially when using generic vascular phantoms.

This retrospective study aims to assess how variations in cerebrovascular geometry and the proximity of the clinical target volume (CTV) to major vessels affect the accumulated dose to CBCs during radiotherapy for brain cancer. It also evaluates the impact of this inter-subject uncertainty on the estimated depletion of CBC.

2. Methods

2.1. Patient selection and data acquisition

Ten GBM patients were selected from the 'Glioma Image Segmentation for Radiotherapy' study (Shusharina and Bortfeld 2020). These patients, treated at Massachusetts General Hospital, Boston between [2015–2022], underwent either intensity-modulated radiation therapy (IMRT) or volumetric modulated arc therapy (VMAT). The selection criteria included CTV size, treatment technique, and tumor location within the brain lobes. The cohort was balanced between the two treatment techniques. Treatment plans and dose distributions were calculated using the RayStation treatment planning system (RayStation, V. 5, 8, and 10). The IMRT treatment plans were built with 6–8 beam angles. The VMAT treatment plans incorporated multiple arcs both coplanar and non-coplanar. The cohort description is given in table 1 and examples of dose distribution are shown in figure 1.

2.2. Inter-subject vascular diversity of the brain

2.2.1. Subject-specific cerebrovascular model

We initially chose 30 MR-angiography (MRA) brain images from the BraVa dataset available on the NITRC repository (www.nitrc.org). After visual checking for consistent anatomical features, we excluded seven images with vascular irregularities or cerebral malformations. The final set of 23 images included 13 males and 10 females, with an average age of 30.2 years (ranging from 19 to 59 years). These images were used to develop multiple brain vessel models (see figure 2).

We used a vessel tracing approach (Hammi 2023), to reconstruct the arterial architecture from the provided SWC files (Ascoli *et al* 2001, Wright *et al* 2013) and extract superficial veins. The major arteries in the datasets are labelled in six categories: the ACAs, middle cerebral arteries (MCAs), and posterior cerebral arteries (PCAs), which supply the frontal, temporal & parietal, and occipital lobes, respectively (Vachha *et al* 2022). The ACAs and MCAs originate from the Circle of Willis (CoW), connecting the left and right internal carotid arteries and the basilar artery (Prabhakaran 2015). The PCAs originate directly from the basilar

Table 1. Overview of the patient cohort selected for this study. The brain lobes are: (frontal cortex lobe (FL), temporal lobe (TL), parietal lobe (PL), proximity to the midline (ML), occipital lobe (OL)).

Patient	CTV size (cm^3)	Tumor location	Treatment technique
P01	242.6	FL/TL	IMRT
P02	366.1	OL (left & right)	IMRT
P03	56.9	FL right	IMRT
P04	465.4	OL (left & right)	IMRT
P05	56.6	TL	IMRT
P06	168.3	FL	VMAT
P07	212.4	FL	VMAT
P08	331.2	PL	VMAT
P09	169.7	ML	VMAT
P10	434.9	FL	VMAT

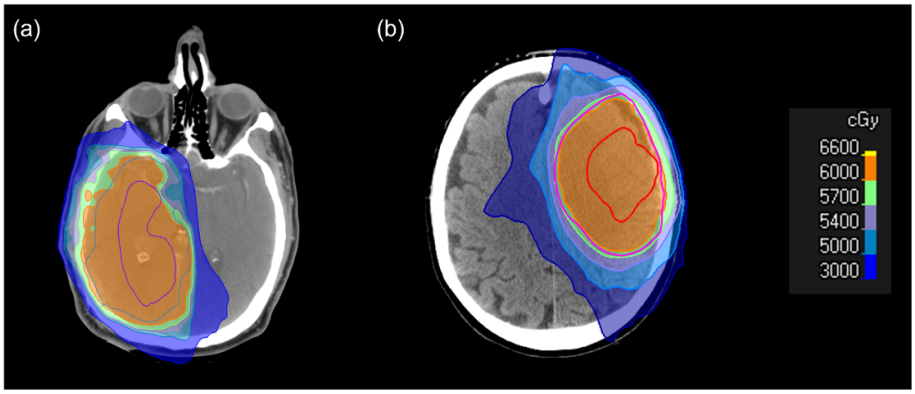

Figure 1. Example dose distributions showing planning strategies for two glioblastoma cases: (a) patient treated with IMRT and (b) patient treated with VMAT.

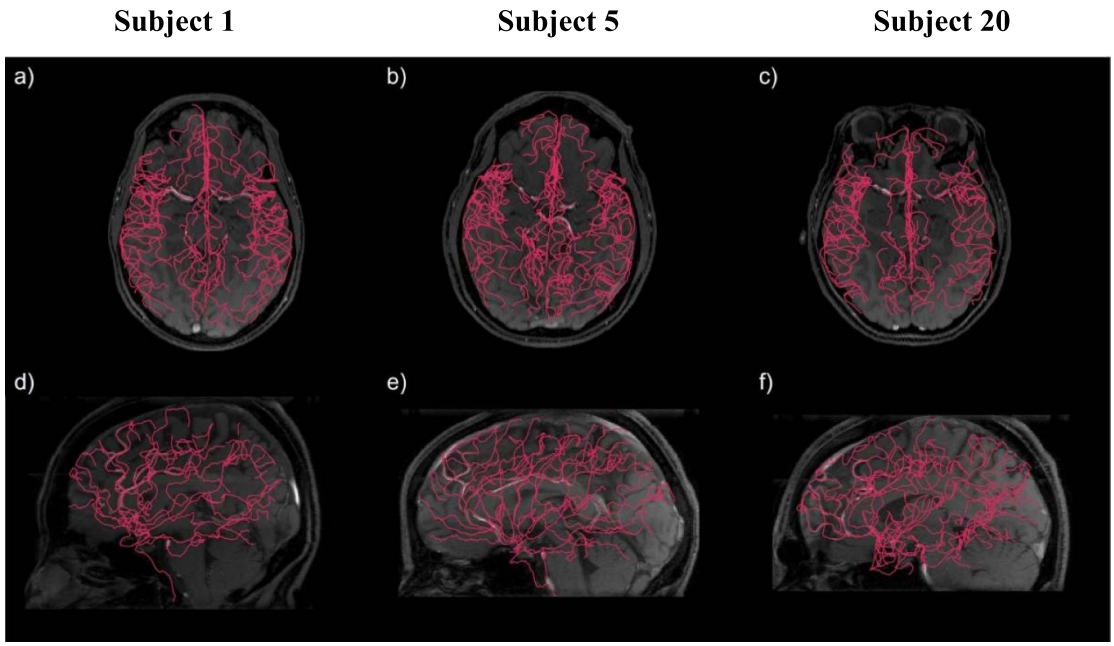

Figure 2. Example of three different arterial branching showing the arterial trees (red solid lines) overlaid on the planar sections of the corresponding MRA images in lateral (upper panel) and transversal (lower panel) directions of the model number 1 (a)–(d), 5 (b)–(e) and 20 (c)–(f), respectively.

artery, which connects to the vertebral arteries. We manually segmented the posterior communicating artery in our models to establish an auxiliary blood supply from the CoW to the PCA. The venous system in our model included superficial veins and dural venous sinuses (superior sagittal, transverse, and sigmoid sinuses).

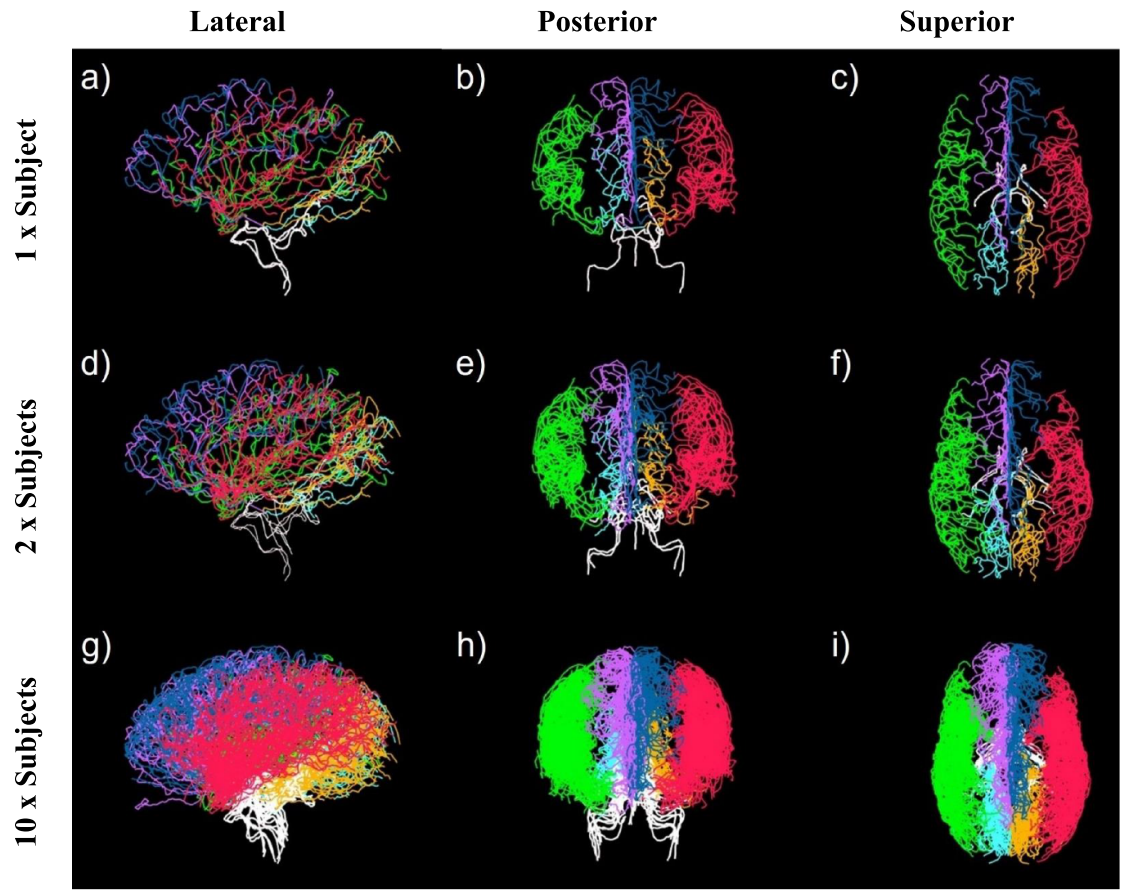

Figure 3. Variability in brain vasculature among subjects: (a)–(c) vascular structures of a single subject, (d)–(f) vascular structures of two subjects, (g)–(i) vascular structures of ten subjects, displayed in lateral, anterior-posterior, and inferior-superior views. The vessels were aligned according to the CoW and basilar artery. Arteries are color-coded as follows: APA (purple/blue), MCA (green/red), and PCA (cyan/orange). The interior carotid and vertebral arteries, as well as the CoW, are shown in white.

Figure 3 illustrates the geometrical variation of major arteries from 10 different subjects. Initially, the 23 realistic blood vessel models were extended using the fractal-based vascular territory approach proposed by Galts and Hammi (2024). This method divides the brain into up to 350 tetrahedral sub-domains, populating each with arterial and venous fractal-like branches. Each fractal trunk bifurcates directly from a realistic vessel and is parametrized by cycle level and the number of daughter branches from a parent branch. The arterial and venous fractals are interconnected to maintain the equilibrium of blood inflow and outflow within the vascular territory.

Each nominal cerebrovascular model (from MRA) was then co-registered with the brain anatomy from the CT images of GBM patients to mimic the inter-model variability in cerebral blood vessels. To ensure a consistent co-registration workflow, we used the 3D Slicer platform to calculate the spatial deformation between MRI and the patient's CT. The resulting displacement field was applied to deform the nominal blood vessels accordingly. In cases where deformable registration did not yield optimal results, we implemented further corrections:

- First, the boundaries between the cranial region and the cortical surface on the CT were segmented based on gray-level features, isolating the brain mass from the surrounding skull.
- The center of mass of the deformed cerebrovascular models was then registered to the brain mass.
- Finally, an affine transformation was performed on the cerebrovascular models to ensure that the peripheral branches of the large blood vessels closely approximated the brain surface without exceeding the boundaries to the cortical surface.

This pipeline was performed for each GBM patient and each nominal cerebrovascular model to create a total of 230 unique cerebrovascular phantom scenarios. The total number of branches was between [3780–8424] branches, with $\sigma = 1110$ branches, underscoring the inter-patient diversity captured by our patient-specific modeling approach (see figure 4).

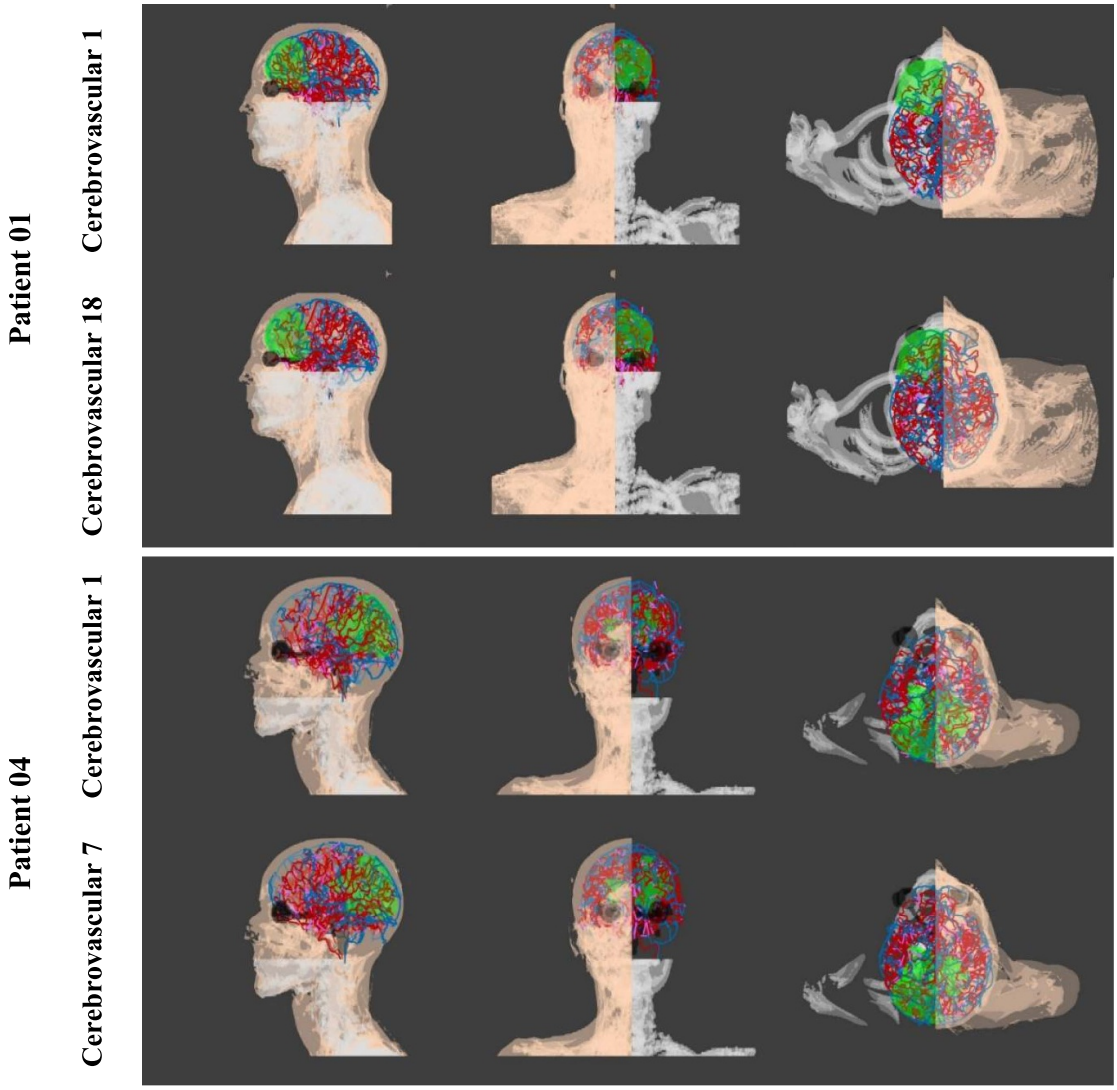

Figure 4. Inter- and intra- subject diversity in blood vessel topography and their spatial relationships with tumors. Cerebrovascular models aligned with the anatomy of two patients. The first two rows (Patient 01) show cerebrovascular models 1 and 18, and the third and fourth rows (Patient 04), depict cerebrovascular models 1 and 7. Each row shows lateral (left), anterior-posterior (middle), and superior-inferior (right) views of one single scenario. The cerebrovascular model contains arteries (red), veins (blue), and capillaries (pink). Tumors are highlighted in green, bones in white, and organs at risk in black.

2.3. Treatment simulation based on dynamic beam delivery

We applied a 4D circulatory system to simulate the blood circulation throughout the body, and explicitly through the blood vessel models of the brain (Hammi 2023). This blood flow model simulates the spatiotemporal distribution of blood particles across 32 different organs. Blood particles, the smallest unit volume for recording dose rates, propagate randomly between bifurcations of the arteries and veins within an organ and between compartments according to the corresponding state transition probability of the hosting organs, which is determined by the hemodynamic parameters of ICRP89 (2002), and depends dynamically on the attenuation time of the blood particles in an organ and their proximity to the corresponding drainage sub-compartments (Hammi 2023). The total number of blood particles varied between subjects due to differences in size and shape of cerebrovascular models. On average, the total blood particle count was $20.6 \times 10^6 \pm 59.1 \times 10^5$ ($\mu \pm \sigma$), with each blood particle having an average volume of 0.27 μl.

A dynamic beam delivery model was implemented to simulate the instantaneous dose rates of a single treatment fraction of 200 cGy. For patients treated with IMRT, the aperture shaping speed was assumed 2.5 cm s^{-1} and for those treated with VMAT, a maximum gantry rotation speed of 6 degrees per second was considered (Rashid *et al* 2021). The dose rates were continuously adjusted based on the incident beam angle.

Dose-volume histograms (DVHs) of the entire blood volume were calculated separately for each patient and each scenario of the cerebral blood vessels. We evaluated the irradiated blood volume ($V_{D>0\,\mathrm{cGy}}$) as a function of the variability of the blood vessel geometry and then compared it to size of the CTV. Various

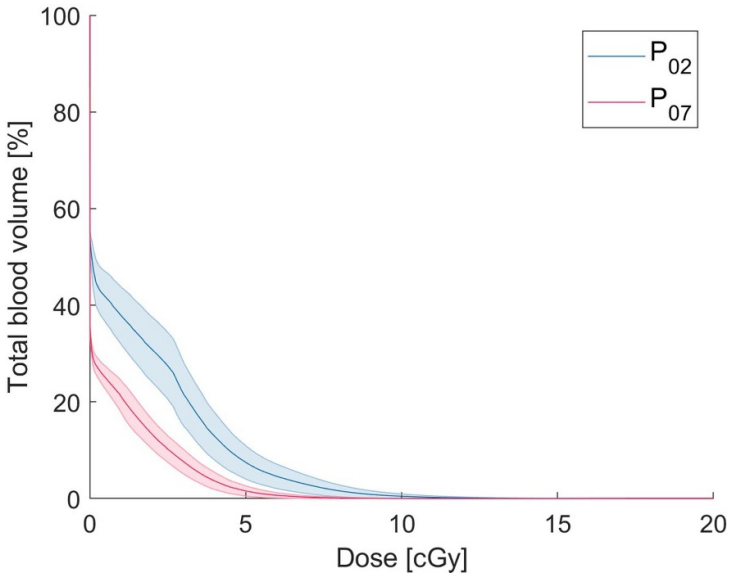

Figure 5. DVH of the total blood volume and the dose uncertainty from inter-subject variation of cerebrovascular geometry of two patients: patient 2 (IMRT) (blue) and patient 7 (VMAT) (red) after a single fraction treatment. The solid lines are the mean values over all scenarios. The shadow area band depicts the 95% confidence interval of the dose dispersion.

DVH indices, such $D_{2\%}$, were evaluated. Additionally, the fraction of killed CBC was estimated for each scenario using in-vitro lymphocyte radiosensitivity parameters (Nakamura *et al* 1990).

3. Results

3.1. DVH analysis

Each dose matrix was separately analyzed for both IMRT and VMAT cohorts, and the resulting DVH and dosimetric indices were calculated. Figure 5 illustrates DVHs for patient 2 (IMRT) and patient 7 (VMAT) after a single treatment fraction of 200 cGy. The DVHs (solid lines) represent average values across 23 morphologically different blood vessels after identical dynamic beam delivery. The shaded areas indicate the 95% confidence intervals ($CI_{95\%}$ from 2.5 to 97.5 percentile), reflecting dose systematic uncertainty across varying cerebrovascular topographies. For both patients, the $CI_{95\%}$ shows a banana-like shape, with lowest uncertainties at both low and high dose regions.

3.2. Inter-model uncertainty in dose indices

Figure 6(a) depicts the uncertainty of $V_{D>0\,\mathrm{cGy}}$ resulting from blood vessel diversity as function of the CTV size. The irradiated blood volume increased with increasing the size of CTV. The CTV size predicted $V_{D>0\,\mathrm{cGy}}$ for IMRT, with an R^2 of 0.998. For VMAT-treated patients, this correlation was less pronounced, with an R^2 of 0.60. For both IMRT and VMAT, the uncertainty in $V_{D>0\,\mathrm{cGy}}$ decreased as the target volume size increased. The highest and lowest $V_{D>0\,\mathrm{cGy}}$ uncertainties observed were (4.5%; 1.4%) and (1.1%; 0.2%) ($CI_{95\%}$) for IMRT and VMAT, respectively.

Figure 6(b) depicts the boxplot of the $D_{2\%}$ index. The interquartile ranges show that IMRT plans are more sensitive to the uncertainty of the blood vessel geometry with respect to the treated region compared to VMAT. The $D_{2\%}$ index dispersion was $CI_{95\%} = \pm 6$ cGy for IMRT plans and $CI_{95\%} = \pm 1$ cGy for VMAT plans.

Figure 7 illustrates the fraction of killed CBC after a single treatment fraction simulation of the corresponding treatment technique as a function of CTV volume. The uncertainty of killed CBC resulting from inter-subject variations of blood vessel increased with CTV volume. For IMRT patients, the highest uncertainty in depleted CBC was $CI_{95\%} \pm 0.25\%$. For VMAT patients, the largest uncertainty was $CI_{95\%} \pm 0.10\%$.

4. Discussion

To the best of our knowledge, this study is the first to highlight the inevitable inter-subject variations in cerebrovascular architecture among radiotherapy patients. This subject variability directly impacts the calculation accuracy of the CBC DVH, affecting the correlation between the treatment plan configuration and the development of RiL in patients.

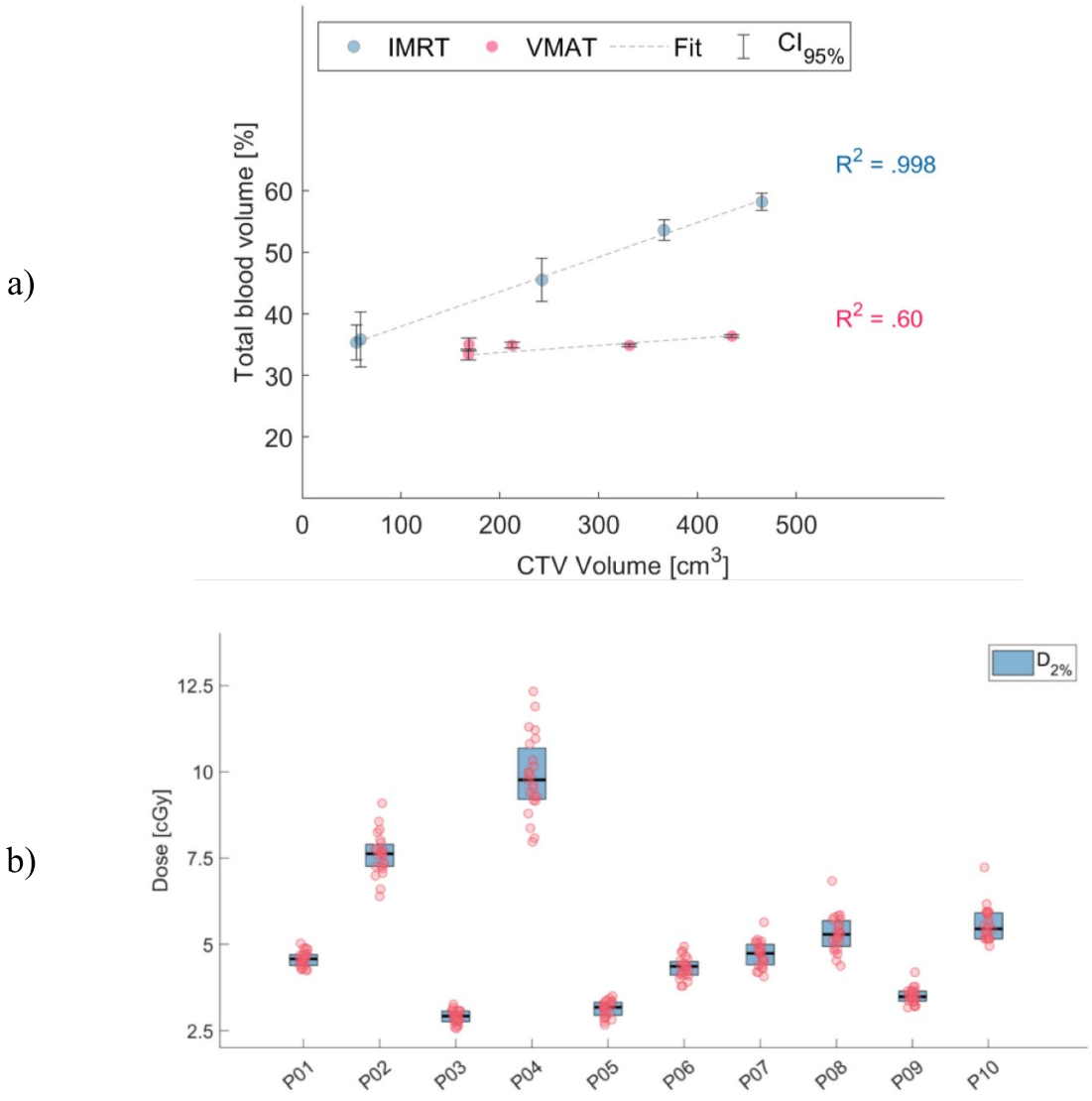

Figure 6. Assessment of dosimetric uncertainty attributed to inter-subject geometric variation of the blood vessel phantom. (a) Uncertainty in $V_{D>0\,cGy}$ Circles represent the mean $V_{D>0\,cGy}$ after one treatment fraction with IMRT (blue) and VMAT (red). Error bars indicate the $CI_{95\%}$. Dashed lines depict the linear regression between $V_{D>0\,cGy}$ and CTV size. (b) box plot of $D_{2\%}$ index with medians (black line), and data points (red circles). The x-axis indicates patient numbers.

Although our brain vessel phantoms were developed from a diverse demographic group, this study only considered the topographic variation of the vessels between subjects. We did not account for other demographic factors such as sex and age, which can also impact the morphology of cerebral vessels and hemodynamic parameters like blood volume and flow rates (ICRP89 2002, Wright *et al* 2013, Yang *et al* 2022). This omission is significant as it directly affects the accumulated dose by the CBC, resulting in differences of up to 4.3% between male and female adults, and up to 10% between male adults and pediatric subjects in low dose regions (Hammi 2023).

Pediatric and female patients have a higher ratio of cardiac output to total body blood volume compared to adult males, at 98.4% and 23.77%, respectively. This leads to a shorter mean transit time of blood particles in the organs compared to adult males. Consequently, the same treatment plan would inherently increase the fraction of blood volume receiving low doses while decreasing the fraction receiving higher doses. This discrepancy could lead to an earlier saturation of the $V_{D>0\,cGy}$ index over fractions, potentially reducing the impact of inter-subject variation in cerebrovascular architecture on the $V_{D>0\,cGy}$ index compared to adult male patients. Conversely, this effect would amplify the impact of the same source of uncertainty on the blood fraction receiving higher doses. A similar effect is expected if the heart rate increases, directly enhancing cardiac output (Hammi 2023).

To better understand the interplay between variability in hemodynamic parameters (heart rate, cardiac output, blood volume) and inter-subject uncertainty of cerebrovascular topography, as well as the impact of

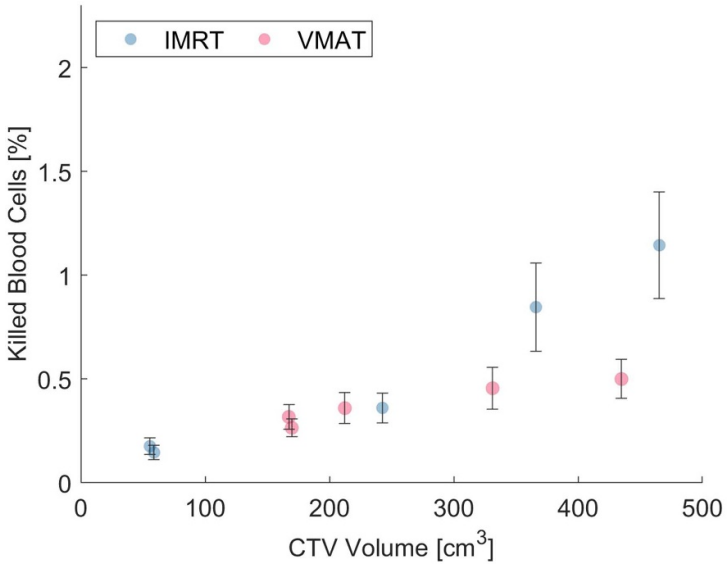

Figure 7. Average fraction of killed CBC for cases listed in table 1, treated with IMRT (blue) and VMAT (red), plotted as a function of CTV volume. Error bars ($CI_{95\%}$) represent the fluctuations due to variability in blood vessel topography.

the different inherent uncertainties that are less patient-specific but arise from the process of plan administration (e.g. patient setup, machine calibration, range error in proton therapy…), further in-depth investigations are necessary. In these studies, a broader scope of uncertainty permutations needs to be evaluated to understand their cumulative intricate impacts on the final DVH of CBC.

$V_{D>0\,\mathrm{cGy}}$ index increased with the CTV size, correlating with the brain volume exposed at any time and the contained blood vessels. Patients 4 (IMRT) and 10 (VMAT) experienced the largest blood pool exposure, with 45.7% ± 9.4% for IMRT and 34.9% ± 1% for VMAT ($\mu \pm \sigma$) after a single treatment fraction. This indicates that the irradiated CBC volume from IMRT plans is more affected by tumor size. Additionally, VMAT delivery is more robust against inter-subject blood vessel variation compared to IMRT delivery. Despite VMAT's larger low-dose bath inherently exposes more branches, its shorter beam delivery time and lower maximum monitor units increase its effective dose rate (Li *et al* 2018), reducing sensitivity to vascular variability.

For both IMRT and VMAT, the estimated number of CBC killed and the associated uncertainty increased with the size of the CTV, consistent with previous studies (Yovino *et al* 2013, Shiraishi *et al* 2018). However, the uncertainty increased more rapidly for IMRT than for VMAT. This difference is primarily due to the distinct beam delivery of the two techniques. IMRT's higher dose rate and greater number of segments lead to higher fluctuations in the exposed volume of CBC and the accumulated dose, particularly when the topography of the blood vessels varies. Additionally, the longer treatment time of IMRT enables more blood particles to recirculate through the dose rate field multiple times, and thus correlates with the uncertainty related to the $D_{2\%}$ index (see figure 7). The coefficient of variation for depleted CBC $\left(\frac{\sigma}{\mu}\right)$ was found to be within 4.3 percentage points (see figure 8), suggesting a negligible dependence on CTV size (Howell 2002). This implies that the observed increase in uncertainty in the number of killed blood cells among patients is mainly due to the increase in the number of irradiated blood cells, which is inherently related to the treatment technique and the treatment plan dose distribution.

Patients 8 and 10 had similar uncertainties in killed CBCs, although patient 8 had a 24% smaller CTV and 4.2% fewer irradiated CBCs. This similarity is due to the fact that patient 8's CTV was located in the parietal lobe, predominantly supplied by the MCA and by the ACA arteries, accounting for approximately 70% of the brain's blood flow (Zarrinkoob *et al* 2015). In addition, the tumor was located near the superior sagittal sinus vein, which drains most of the brain's blood, therefore, the accumulated dose to CBC flowing through the CTVs in this part of the brain is more sensitive to inter-subject variability.

The overall uncertainty of depleted CBC was 11.2% (1σ of the mean). These findings suggest that accounting for cerebrovascular variability would provide insight on whether a deeper analysis can be relevant. Given the complexities of developing personalized cerebral vessel models from standard imaging in cancer patients, it is recommended to consider these uncertainties in fractionated radiotherapy studies. Additionally, accounting for treatment technique-specific uncertainties could help select the optimal radiation therapy technique for individual patients to minimize RiL.

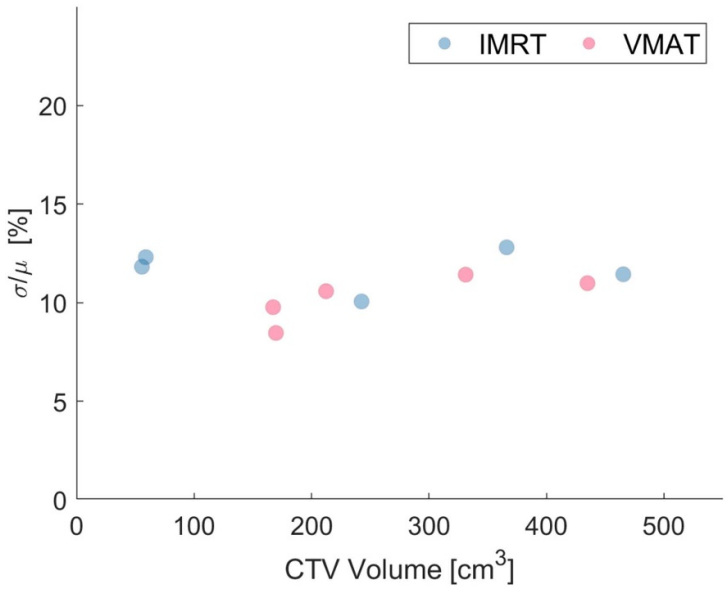

Figure 8. Coefficient of variation for the data presented in figure 6(b).

While this study focused on GBM patients and conventional radiotherapy, the findings have broader implications for other intracranial tumors and head and neck regions. The blood vessels supplying these regions, like the internal carotid and jugular veins, were included in our hybrid cerebrovascular models. Future studies are needed to explore other treatment modalities such as proton therapy, and to understand how the lack of personalized vascular anatomy affects the precision of RiL estimation in charge particle therapy.

5. Conclusion

Inter-subject variability in cerebrovascular topography is inevitable and it introduces an additional layer of uncertainty in studies that use less patient-specific blood vessel phantoms to calculate the radiation dose to circulating immune cells. VMAT delivery showed better robustness to these uncertainties compared to IMRT. We recommend that studies investigating RiL consider these uncertainties to improve the accuracy of their assessments.

Data availability statement

The data cannot be made publicly available upon publication because they are owned by a third party and the terms of use prevent public distribution. The data that support the findings of this study are available upon reasonable request from the authors.

ORCID iDs

Abdelkhalek Hammi https://orcid.org/0000-0002-4001-1180
Nadya Shusharina https://orcid.org/0000-0003-3041-2551

References

Ascoli G A, Krichmar J L, Nasuto S J and Senft S L 2001 Generation, description and storage of dendritic morphology data *Phil. Trans. R. Soc.* B **356** 1131–45

Basler L, Andratschke N, Ehrbar S, Guckenberger M and Tanadini-Lang S 2018 Modelling the immunosuppressive effect of liver SBRT by simulating the dose to circulating lymphocytes: an in-silico planning study *Radiat. Oncol.* **13** 10

Byun H K 2019 Clinical predictors of radiation-induced lymphopenia in patients receiving chemoradiation for glioblastoma: clinical usefulness of intensity-modulated radiotherapy in the immuno-oncology era *Radiat. Oncol.* **14** 51

Daneman R and Prat A 2015 The blood-brain barrier *Cold Spring Harb. Perspect. Biol.* **7** a020412

Galts A and Hammi A 2024 FLASH radiotherapy sparing effect on the circulating lymphocytes in pencil beam scanning proton therapy: impact of hypofractionation and dose rate *Phys. Med. Biol.* **69** 025006

Grossman S A, Ellsworth S, Campian J, Wild A T, Herman J M, Laheru D, Brock M, Balmanoukian A and Ye X 2015 Survival in patients with severe lymphopenia following treatment with radiation and chemotherapy for newly diagnosed solid tumors *Natl Compr. Cancer Netw.* **13** 1225–31

Hammi A 2023 4D dosimetric-blood flow model: impact of prolonged fraction delivery times of IMRT on the dose to the circulating lymphocytes *Phys. Med. Biol.* **68** 145017

Hammi A, Paganetti H and Grassberger C 2020 4D blood flow model for dose calculation to circulating blood and lymphocytes *Phys. Med. Biol.* **65** 055008

Howell D 2002 *Statistical Methods for Psychology* (Wiley)

ICRP89 2002 Basic anatomical and physiological data for use in radiological protection reference values *Ann. ICRP* **32** 89

Ilic I and Ilic M 2023 International patterns and trends in the brain cancer incidence and mortality: an observational study based on the global burden of disease *Heliyon* **9** e18222

Jin J Y, Gu A, Wang W, Oleinick N L, Machtay M and Spring Kong F M 2020 Ultra-high dose rate effect on circulating immune cells: a potential mechanism for FLASH effect? *Radiother. Oncol.* **149** 55–62

Kim W J, Dho Y S, Ock C Y, Kim J W, Choi S H, Lee S T, Kim I H, Kim T M and Park C K 2019 Clinical observation of lymphopenia in patients with newly diagnosed glioblastoma *J. Neurooncol.* **43** 321–8

Kleinberg L, Sloan L, Grossman S and Lim M 2019 Radiotherapy, lymphopenia, and host immune capacity in glioblastoma: a potentially actionable toxicity associated with reduced efficacy of radiotherapy *Neurosurgery* **85** 441–53

Li Y, Wang J, Tan L, Hui B, Ma X, Yan Y, Xue C, Shi X, Drokow E K and Ren J 2018 Dosimetric comparison between IMRT and VMAT in irradiation for peripheral and central lung cancer *Oncol. Lett.* **15** 3735–45

Mapunda J A, Tibar H, Regragui W and Engelhardt B 2022 How does the immune system enter the brain? *Front. Immunol.* **13** 805657

Nakamura N, Kusunoki Y and Akiyama M 1990 Radiosensitivity of CD4 or CD8 positive human T-lymphocytes by an in vitro colony formation *Radiat. Res.* **123** 224–7

Ostrom Q T, Price M, Neff C, Cioffi G, Waite K A, Kruchko C and Barnholtz-Sloan J S 2017 CBTRUS statistical report: primary brain and other central nervous system tumors diagnosed in the United States in 2010–2014 *Neuro Oncol.* **19** v1–v88

Pillay J, Tak T, Kamp V M and Koenderman L 2013 Immune suppression by neutrophils and granulocytic myeloid-derived suppressor cells: similarities and differences *Cell. Mol. Life Sci.* **70** 3813–27

Prabhakaran S 2015 Imaging markers of stroke risk in asymptomatic carotid artery stenosis *Brain Circ.* **1** 38–46

Rashid A, Ahmad Z, Memon M A and Hashim A S M 2021 Volumetric modulated arc therapy (VMAT): a modern radiotherapy technique—a single institutional experience *Pak. J. Med. Sci.* **37** 355–61

Razavi S M, Lee K E, Jin B E, Aujla P S, Gholamin S and Li G 2016 Immune evasion strategies of glioblastoma *Front. Surg.* **3** 11

Saeed A B 2024 Systematic review and pooled analysis of the impact of treatment-induced lymphopenia on survival of glioblastoma patients *Radiat. Oncol.* **19** 36

Shalom D E, Trevisan M A, Mallela A, Nuñez M and Goldschmidt E 2021 Brain folding shapes the branching pattern of the middle cerebral artery *PLoS One* **16** e0245167

Shin J *et al* 2021 HEDOS-a computational tool to assess radiation dose to circulating blood cells during external beam radiotherapy based on whole-body blood flow simulations *Phys. Med. Biol.* **66** 164001

Shiraishi Y *et al* 2018 Severe lymphopenia during neoadjuvant chemoradiation for esophageal cancer: a propensity matched analysis of the relative risk of proton versus photon-based radiation therapy *Radiother. Oncol.* **128** 154–60

Shusharina N, Söderberg J, Edmunds D, Löfman F, Shih H and Bortfeld T 2020 Automated delineation of the clinical target volume using anatomically constrained 3D expansion of the gross tumor volume *Radiat. Oncol.* **146** 37–43

Song A J 2021 Impact of lymphopenia on survival for elderly patients with glioblastoma: a secondary analysis of the CCTG CE.6 (EORTC 26062–22061, TROG03.01) randomized clinical trial *Neurooncol. Adv.* **3** vdab153

Tregub P P, Averchuk A S, Baranich T I, Ryazanova M V and Salmina A B 2022 Physiological and pathological remodeling of cerebral microvessels *Int. J. Mol. Sci.* **23** 12683

Vachha B A, Massoud T F and Huang S Y 2022 Anatomy of the cerebral cortex, lobes, and cerebellum *Neuroimaging Clin. North Am.* **32** 463–73

Wright S N, Kochunov P, Mut F, Bergamino M, Brown K M, Mazziotta J C, Toga A W, Cebral J R and Ascoli G A 2013 Digital reconstruction and morphometric analysis of human brain arterial vasculature from magnetic reconstruction and morphometric analysis of human brain arterial vasculature from magnetic resonance angiography *NeuroImage* **82** 170–81

Yang A C *et al* 2022 A human brain vascular atlas reveals diverse mediators of Alzheimer's risk *Nature* **603** 885–92

Yovino S, Kleinberg L, Grossman S A, Narayanan M and Ford E 2013 The etiology of treatment-related lymphopenia in patients with malignant gliomas: modeling radiation dose to circulating lymphocytes explains clinical observations and suggests methods of modifying the impact of radiation on immune cells *Cancer Invest.* **31** 140–4

Zarrinkoob L, Ambarki K, Wåhlin A, Birgander R, Eklund A and Malm J 2015 Blood flow distribution in cerebral arteries *J. Cereb. Blood Flow Metab.* **35** 648–54